Electronic Supplementary Information (ESI) for:

Nitrogen and Phosphorus Modification to Enhance the Catalytic Activity of Biomass-Derived Carbon toward Oxygen Reduction Reaction

Lei Han,[a] Xingyu Cui,[a] Yanyan Liu,[b*] Guosheng Han,[a] Xianli Wu,[a*] Chunbao (Charles) Xu,[c, d] and Baojun Li[a]

[a] Research Center of Green Catalysis, College of Chemistry, Zhengzhou University, 100 Science Road, Zhengzhou 450001, P. R. China

[b] Institute of Chemical Industry of Forest Products, CAF; National Engineering Lab. for Biomass Chemical Utilization; Key Lab. of Chemical Engineering of Forest Products, National Forestry and Grassland Administration; Key Lab. of Biomass Energy and Material, Jiangsu Province; Co-Innovation Center of Efficient Processing and Utilization of Forest Resources, Nanjing 210042, P. R. China

[c] College of Chemical Engineering, Zhengzhou University, 100 Science Road, Zhengzhou 450001, P. R. China

[d] Department of Chemical & Biochemical Engineering, Western University, London, Ontario, Canada

[*] Corresponding Author. E-mail: lyylhs180208@163.com (Y.Y. Liu), and wuxianli@zzu.edu.cn (X. L. Wu)

Total number of pages: 10
Total number of figures: 12
Total number of table: 2

Table of Contents

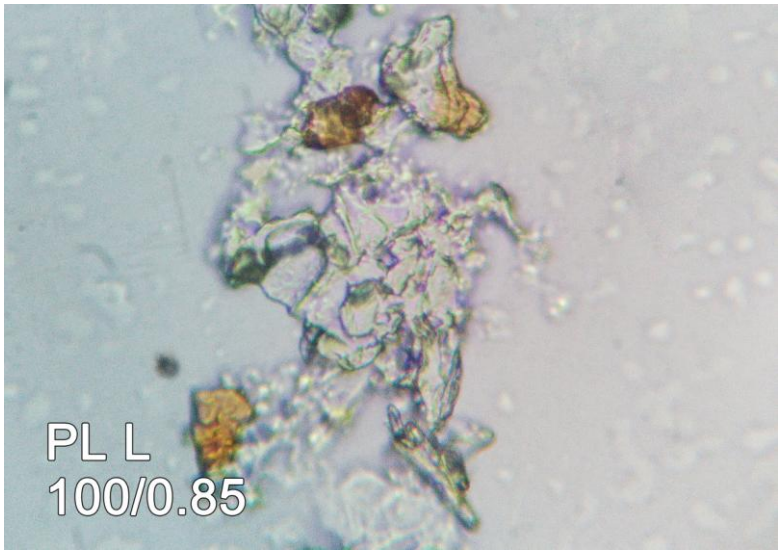

Figure S1. Optical microscope image of Fructus azedarach.

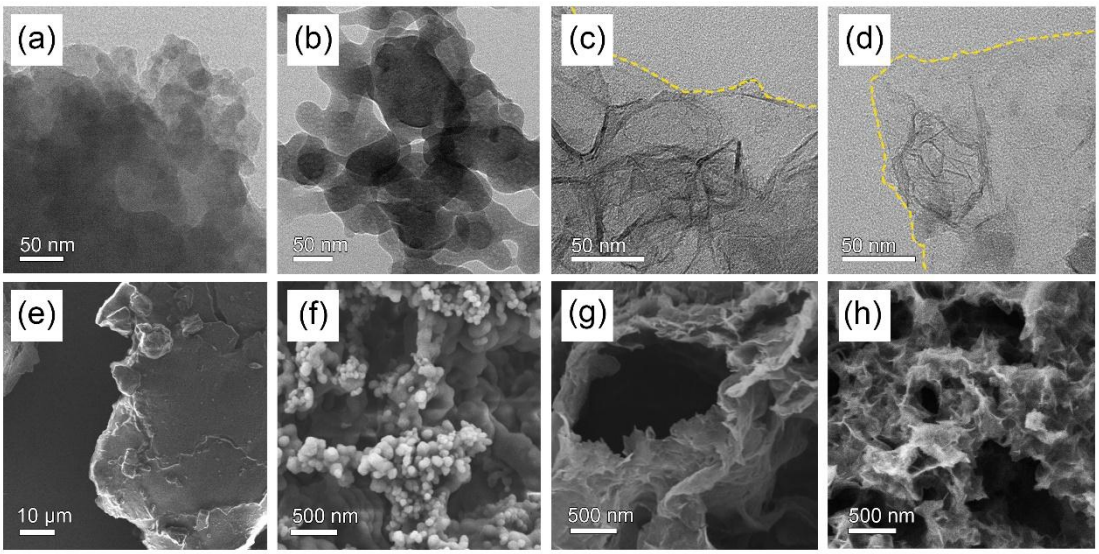

Figure S2. (a) TEM image of Fructus azedarach, (b) TEM image of PTC, (c) TEM image of KAC, (d) TEM image of NPDC-1.09, (e) SEM image of Fructus azedarach, (f) SEM image of PTC, (g) SEM image of KAC, and (h) SEM image of NPDC-1.09.

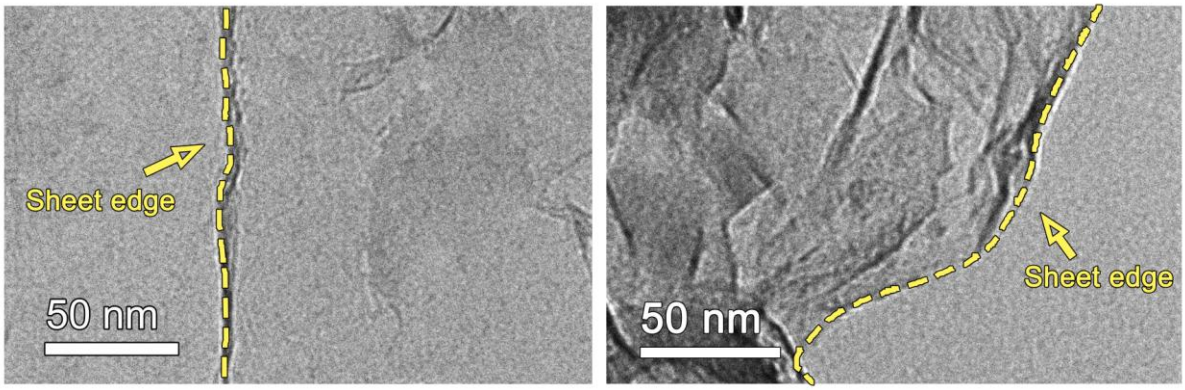

Figure S3. (a) TEM image of NPDC-1.09, (b) TEM image of hydrothermally treated NPDC (NPDC-H).

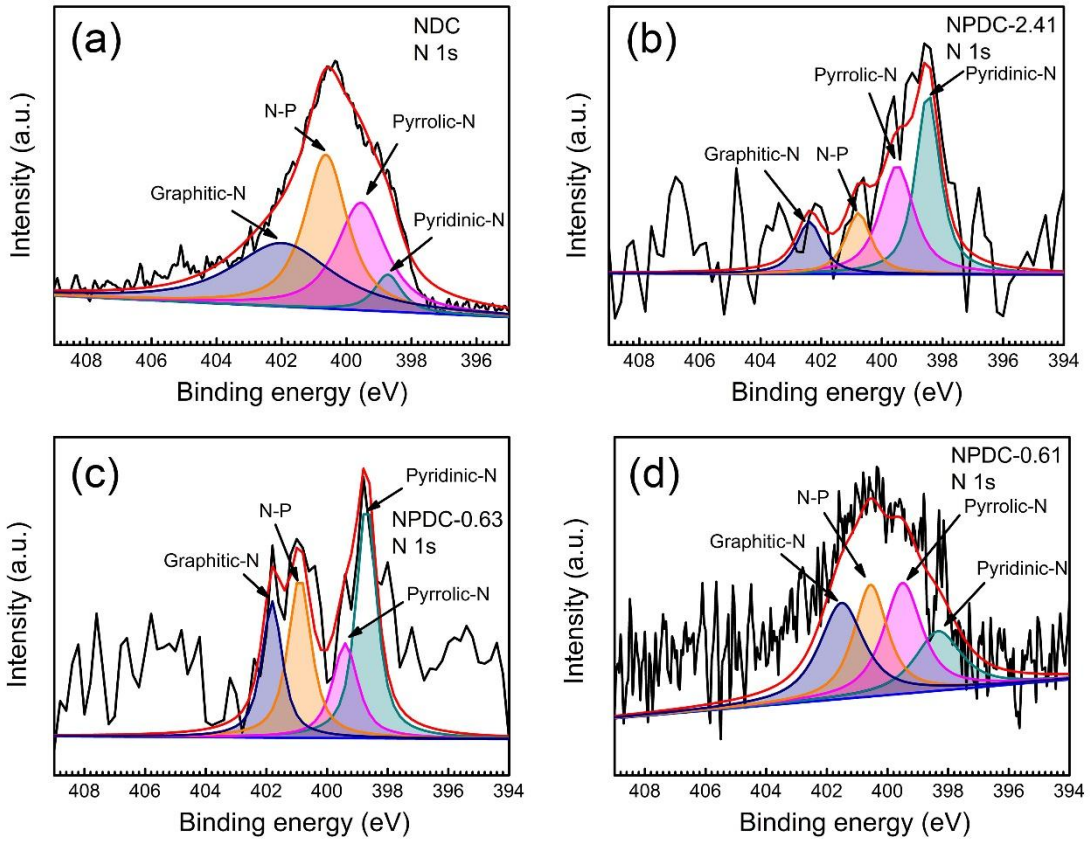

Figure S4. High resolution XPS spectra of N 1s in (a) NDC, (b) NPDC-2.41, (c) NPDC-0.63, and (d) NPDC-0.61.

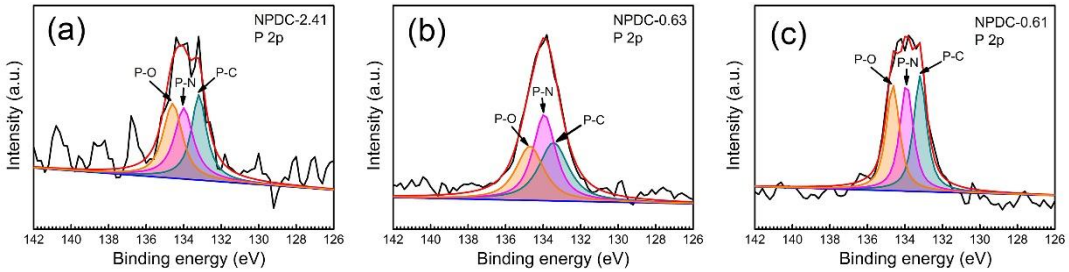

Figure S5. High resolution XPS spectra of P 2p in (a) NPDC-2.4, (b) NPDC-0.63, and (c) NPDC-0.61.

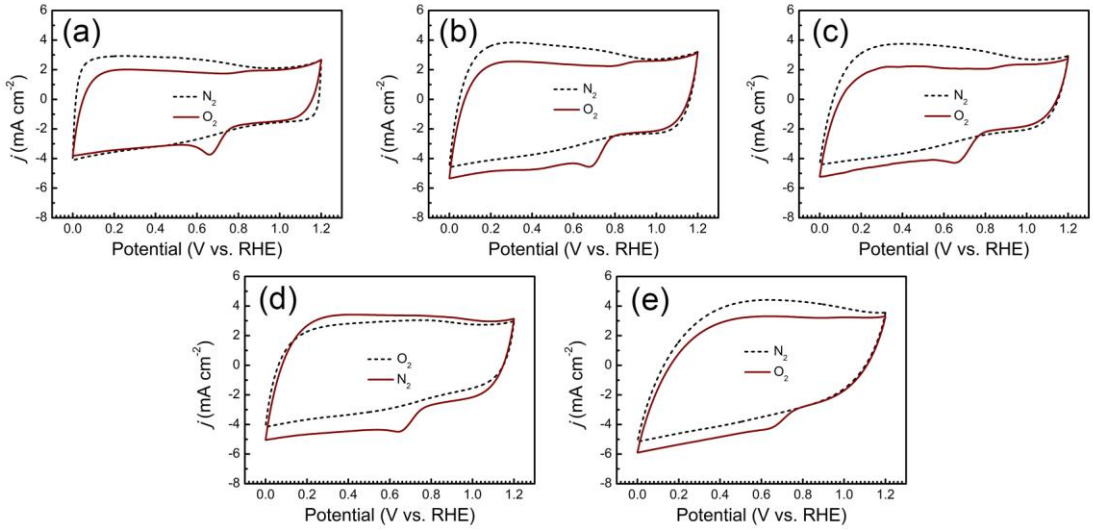

Figure S6. CV curve in (a) NDC, (b) NPDC-0.61, (c) NPDC-0.63, (d) NPDC-2.41, (e) NPDC-H.

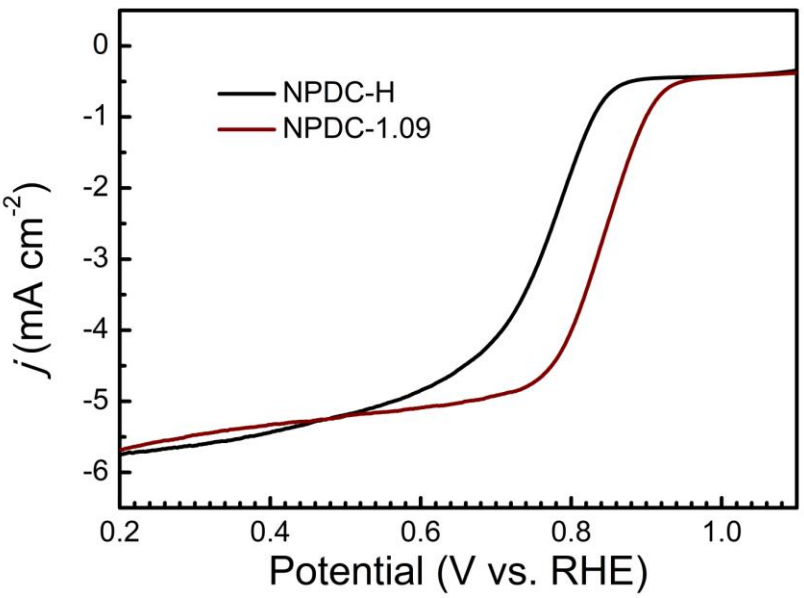

Figure S7. LSV curve of NPDC-H and NPDC-1.09.

Table S1. N 1s and P 2p fitted results of all sample.

Samples	Nitrogen (%)				Phosphorous (%)		
	Pyridine	Pyrrolic	N-P	Graphite	P-O	P-N	P-C
KAC	12.25	55.63	--	32.12	--	--	--
NDC	5.21	27.45	34.38	32.96	--	--	--
NPDC-2.41	39.86	33.69	14.24	12.21	34.13	32.17	32.89
NPDC-1.09	44.83	22.03	14.57	18.57	25.52	32.14	42.34
NPDC-1.09 (ar)	14.52	26.20	27.76	31.52	26.54	37.91	35.55
NPDC-0.63	52.17	14.50	20.29	13.04	34.23	38.30	27.47
NPDC-0.61	20.28	28.32	21.11	30.29	34.24	33.93	31.83

*PS: (ar) means after reaction.

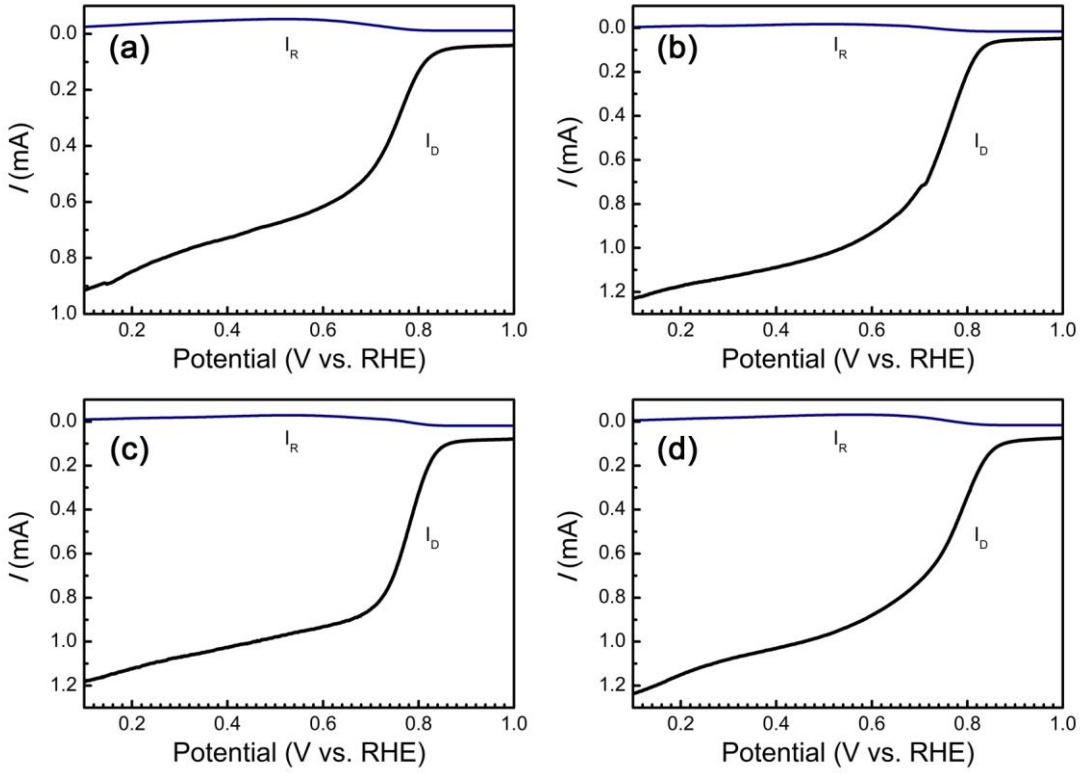

Figure S8. (a) Disk and ring currents of NDC, (b) Disk and ring currents of NPDC-0.61, (c) Disk and ring currents of NPDC-0.63, (d) Disk and ring currents of NPDC-2.41.

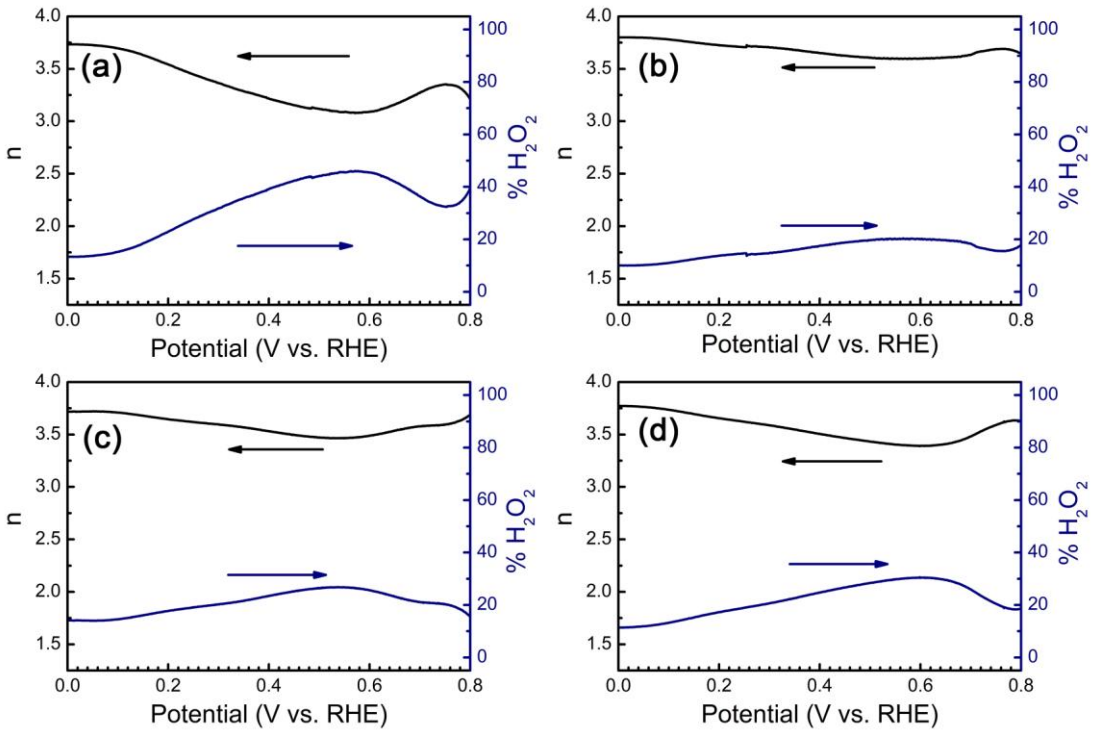

Figure S9. (a-d) Calculated n and determined % H_2O_2 at various potentials of NDC, NPDC-0.61, NPDC-0.63 and NPDC-2.41.

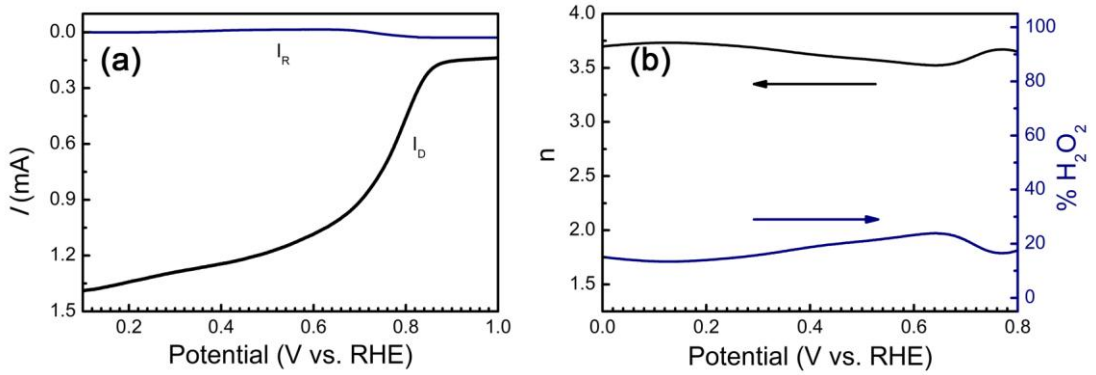

Figure S10. (a) Disk and ring currents of NPDC-H, (b) Calculated n and determined % H_2O_2 of NPDC-H.

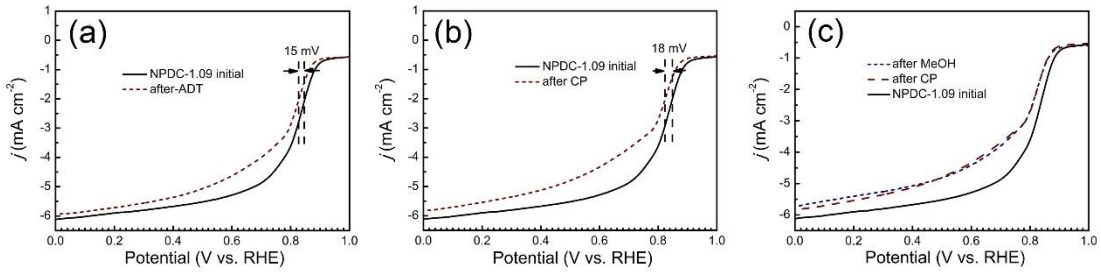

Figure S11. (a) LSV diagram of NPDC-1.09 after ADT test, (b) LSV diagram of NPDC-1.09 after CP test, and (c) LSV diagram of NPDC-1.09 after adding MeOH.

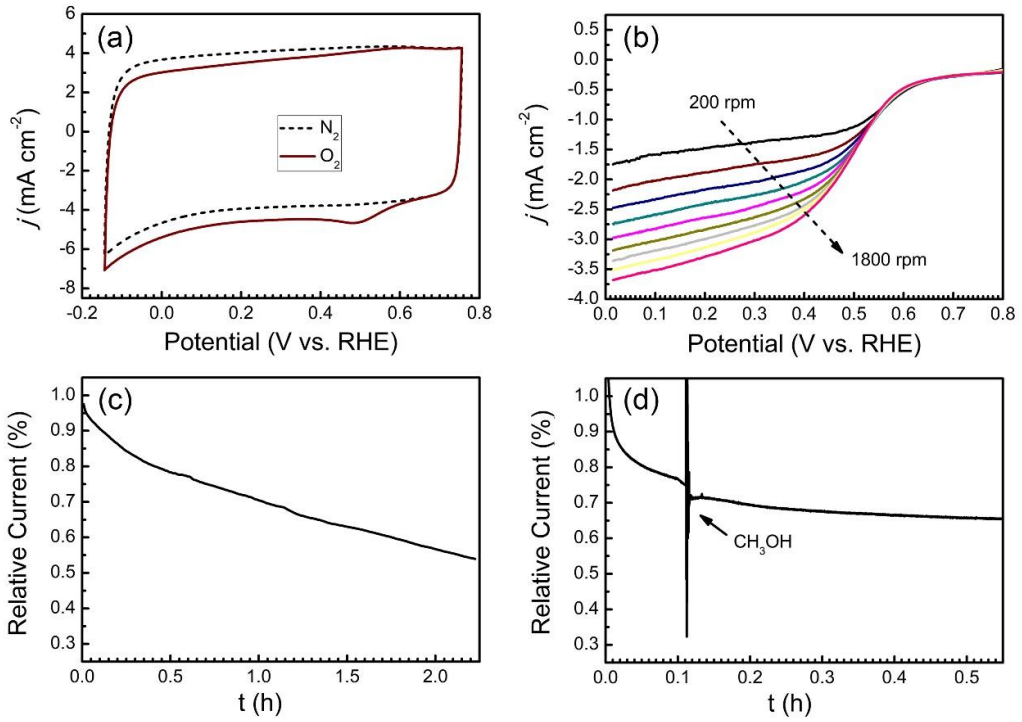

Figure S12. (a) CV curves NPDC-1.09 in 0.1 M $HClO_4$, (b) LSV curves of NPDC-1.09 with rotate speed of 200 rpm-1800 rpm in 0.1 M $HClO_4$; (c) the CP curve on NPDC-1.09 in 0.1 M $HClO_4$, and (d) the CP curve on NPDC-1.09 with addition of MeOH in 0.1 M $HClO_4$.

Table S2. The performance of the sample NPDC-1.09 in this work is compared with the samples in other papers.

Biomass source	**Heteroatom precursor**	**Other precursors**	**Synthesis strategy**	**Surface area [m^2 g^{-1}]**	E_{onset} **[V]**	$E_{1/2}$ **[V]**	E_{OER} **[V]**	**Transferred electrons (*n*)**	**Zn-air battery cycle duration [h]**	**Ref.**
Sodium alginate	2-methylimidazole (N)	$Co(NO_3)_2$ $NaHCO_3$	Activation, MOF growth	252	0.90	0.83	–	4.3	–	S1
Peanut-shell	Dopamine (N)	$Co(AC)_2$ $Fe(NO_3)_3$ KOH	Activation, Pyrolysis	1863	1.05	0.84	1.61	4.8	155	S2
D-Glucose and Cellulose	Soya bean flour (N)	–	Pyrolysis Hydrothermal	449	0.90	0.76	–	3.8	–	S3
Hair	Self-doping (N, S)	KOH	Pyrolysis, Activation	1698	0.92	0.82	–	3.9	–	S4
Coconut shell	Urea (N) Phosphate acid (P)	–	Activation, Pyrolysis	1216	0.94	0.75	–	3.7	–	S5
Triarrhena	Melamine	KOH	Pyrolysis Hydrothermal	1347	0.94	0.83	–	3.8	–	S6
Pristine catkin	NH_3 (N)	[Omim]$FeCl_4$	Pyrolysis	385	0.93	0.85	1.54	4	–	S7

Wood	NH_4Cl (N)	–	Pyrolysis Cellulose Activation	1039	0.99	0.83	1.61	3.9	80	S8
Peach gum	Melamine (N)	$Co(NO_3)_2$	Pyrolysis	-	0.91	0.81	1.63	3.9	32	S9
Porphyra	Self-doping (N, S)	$FeCl_3$	Encapsulate, Pyrolysis	1533	0.96	0.84	1.62	3.8	66.5	S10
Fructus azedarach	$NH_4H_2PO_4$ (N, P) Cyanamide (N)	$KHCO_3$	Pyrolysis, Activation Hydrothermal	1584	0.94	0.84	1.68	3.9	84	This work

REFERENCES

S1. J. H. Shu, Q. J. Niu, N. N. Wang, J. Niu, G. P. Ma, Alginate derived Co/N doped hierarchical porous carbon microspheres for efficient oxygen reduction reaction. *Appl. Surf. Sci.*, 2018, **485**, 520–528. DOI: 10.1016/j.apsusc.2019.04.204

S2. J. J. Liu, T. He, Q. C. Wang, Z. X. Zhou, Y. Q. Zhang, H. Q. Wu, Q. Li, J. Zheng, Z. F. Sun, Y. P. Lei, J. M. Ma, Y. Zhang, Confining ultrasmall bimetal alloys in porous N-carbon as scalable and sustainable electrocatalysts for rechargeable Zn–air batteries. *J. Mater. Chem. A*, 2019, **7**, 12451–12456. DOI: 10.1039/C9TA02264C

S3. S. M. Alatalo, K. P. Qiu, K. Preuss, A. Marinovic, M. Sevilla, M. Sillanpaa, X. Guo, M. M. Titirici, Soy protein directed hydrothermal synthesis of porous carbon aerogels for electrocatalytic oxygen reduction. *Carbon*, 2015, **96**, 622–630. DOI: 10.1016/j.carbon.2015.09.108

S4. K. N. Chaudhari, M. Y. Song, J. S. Yu, Transforming hair into heteroatom-doped carbon with high surface area. *Small*, 2014, **12**, 2625–2636. DOI: 10.1002/smll.201303831

S5. M. Boighei, N. Laocharoen,; E. Kibena-Poldsepp, L. Johansson, Porous N,P-doped carbon from coconut shells with high electrocatalytic activity for oxygen reduction: Alternative to Pt-C for alkaline fuel cells. *Appl. Catal. B*, 2017, **204**, 394–402. DOI: 10.1016/j.apcatb.2016.11.029

S6. P. P. Chen, J. B. Zang, S. Y. Zhou, S. P. Jia, P. F. Tian, H. X. Cai, H. W. Gao, Y. H. Wang, N-doped 3D porous carbon catalyst derived from biowaste Triarrhena sacchariflora panicle for oxygen reduction reaction. *Carbon*, 2019, **146**, 70–77. DOI: 10.1016/j.carbon.2019.01.106

S7. G. P. Liu, B. Wang, P. H. Ding, Y. Z. Ye, W. X. Wei, W. S. Zhu, L. Xu, J. X. Xia, H. M. Li, Reactable ionic liquid in situ-induced synthesis of Fe_3O_4 nanoparticles modified N-doped hollow porous carbon microtubes for boosting multifunctional electrocatalytic activity. *J. Alloys Compd.*, 2019, **797**, 849–858. DOI: 10.1016/j.jallcom.2019.04.284

S8. X. W. Peng, L. Zhang, Z. X. Chen, L. X. Zhong, D. K. Zhao, X. Chia, X. W. Zhao, L. G. Li, X. H. Lu, K. Leng, C. B. Liu, W. Liu, W. Tang, K. P. Loh, Hierachically porous carbon plates derived from wood as bifunctional ORR/OER electrodes. *Adv. Mater.*, 2019, **07**, 1900341–1900348. DOI: 10.1002/adma.201900341

S9. Y. H. Tian, L. Xu, J. Bao, J. C. Qian, H. N. Su, H. M. Li, H. D. Gu, C. Yan, H. N. Li, Hollow cobalt oxide nanoparticles embedded in nitrogen-doped carbon nanosheets as an efficient bifunctional catalyst for Zn-air battery. *J. Energ. Chem.*, 2019, **33**, 59–66. DOI: 10.1016/j.jechem.2018.08.007

S10. J. T. Zhang, M. Zhang, Y. Zeng, J. S. Chen, Li. X. Qiu, H. Zhou, C. J. Sun, Y. Yu, C. Z. Zhu, Z. H. Zhu, Single Fe atom on hierarchically porous S, N-codoped nanocarbon derived from porphyra enable boosted oxygen catalysis for rechargeable Zn-air batteries. *Small*, 2019, **15**, 1900307–1900318. DOI: 10.1002/smll.201900307